04/20/06
TD-06-017

Nb_3Sn Strand Quench Current Estimate Based on Adiabatic models

B. Bordini and S. Feher

This note describes adiabatic models which can faithfully characterize the measured quench behavior of Nb3Sn strands with extremely low RRR value. Two major instability mechanisms – magnetization and self field - have been considered and implemented as a source of the heat generation. Both mechanisms have been applied separately and jointly to compare their predictions with experimental data.

INDEX:

1 Introduction

For the past year several Nb_3Sn strands quench behavior was extensively studied [1]-[3] using a special Voltage Spike Detection System (VSDS) and several different measurement techniques to shed light on conductor instabilities. Two different types of instability mechanisms were observed depending on the experimental conditioning of the sample. Starting the current ramp when the sample was not magnetized we obtained different VSDS signal shapes and quench current values as a function of the external magnetic field compare to the case when the sample was strongly magnetized which was achieved by ramping up the magnetic field at fixed current values until the sample has quenched.

In order to model this quench behavior of the strand two instability mechanisms were considered: self field instability and magnetization instability. Modeling both instability mechanisms have the following assumptions. The potential energy stored in the superconductor due to self field or magnetization is released instantaneously (adiabatic approach). This modeling approach is an integral method which will assume that once the flux jump mechanism starts it will continue until the total stored energy have been released.

The released energy will warm up the superconductor (no escape of heat will be assumed) and if the temperature is high enough that the superconductor can not carry, with a negligible electrical resistivity, the transport current it will quench.

In chapter 2 the strand geometrical dimensions and detailed material properties will be described which are used in the model. Chapter 3 and 4 will summarize the magnetization stored energy and self field stored energy calculations respectively. In chapter 5 the enthalpy calculation is described and the way how the model calculates the quench current value. In Chapter 6 and 7 the obtained results are described. Chapter 8 and 9 describe the effect of the magnetization produced by the self-field. In chapter 10 the model is compared with experimental data.

2. Strand geometrical and material properties

2.1 Geometry of the 1mm MJR

The MJR strand cross section, fig. 2.1.1, is composed by three regions: a central copper rod, a composite zone and an external copper shell. The composite region is made of hexagonal sub-elements; in our case the number of sub-elements is 54 (12 in the first, 18 in the second and 24 in the third layer). After the heat treatment of the strand, each sub-element has a central part made of bronze surrounded by Nb_3Sn. This part of the sub-element will be named 'filament'; the filament area is generally named 'non-copper area'.
The external part of the sub-element is a thin copper layer which separates the filaments fro each other.

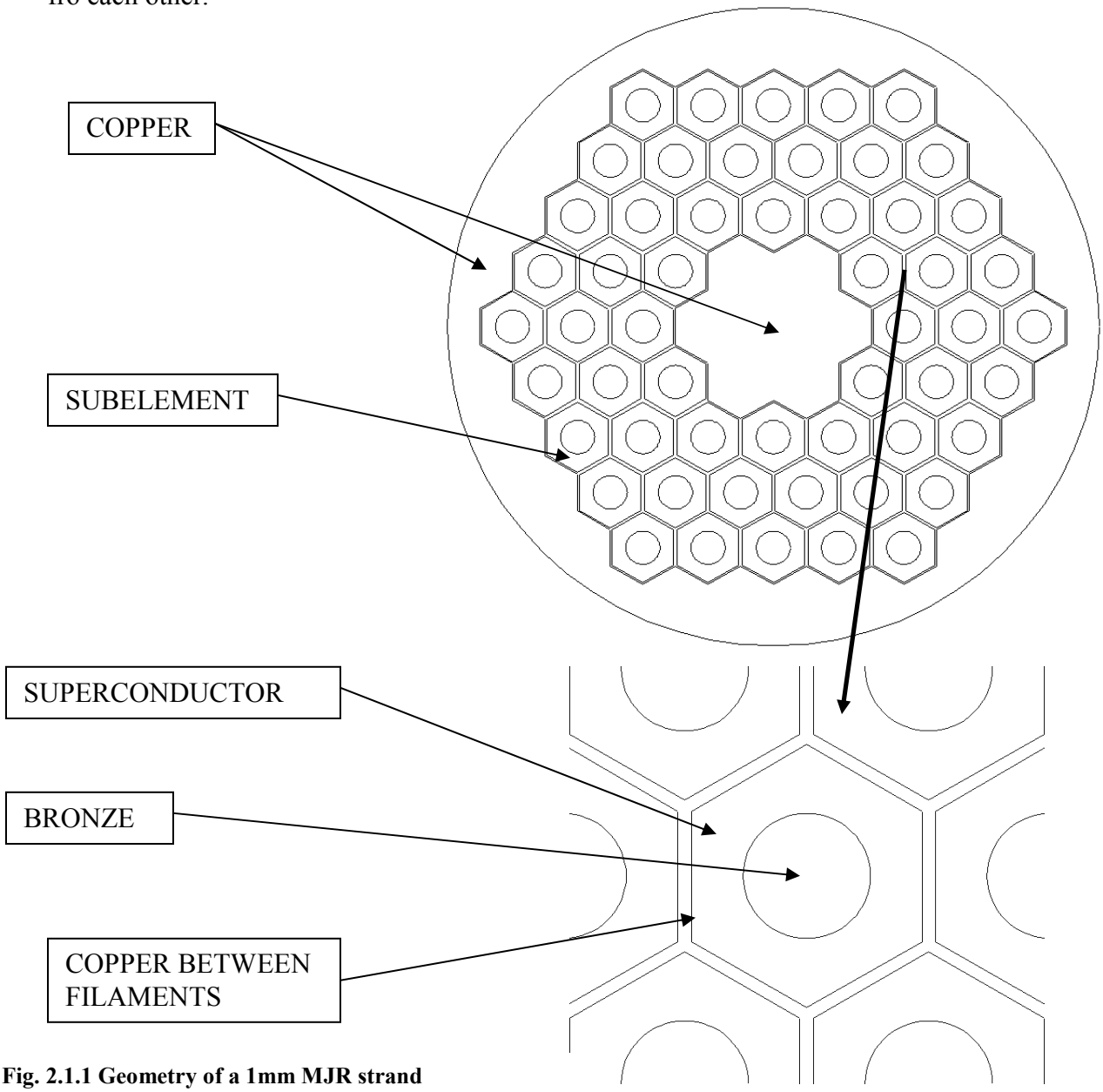

Fig. 2.1.1 Geometry of a 1mm MJR strand

The area values for the different parts in the strand cross section are shown in tab. 2-1.

Tab. 2-1 Areas in mm^2

Non-Cu	Sub-elements	Nb_3Sn	bronze	Cu sub-elements	Cu rod	Cu shell
0.422	0.474	0.305	0.117	0.052	0.0615	0.250

The model, presented latter in the note, takes into account only the composite region. This region is approximated with an area within two circles (external and internal radius named to R and R_f respectively), fig.2.1.2. These values have been established using the following criteria:

$$\pi R_f^2 = Cu\_Rod\_Area \quad \rightarrow \quad R_f = 0.14[mm]$$

$$\pi\left(R^2 - R_f^2\right) = Sub-elements\_Area \quad \rightarrow \quad R = 0.413[mm]$$

Another relevant parameter for the model is the ratio, λ, between the non copper area and the total area of the composite. For our geometry:

$$\lambda = \frac{Non-Cu\_area}{Sub-elements\_area} = 0.89$$

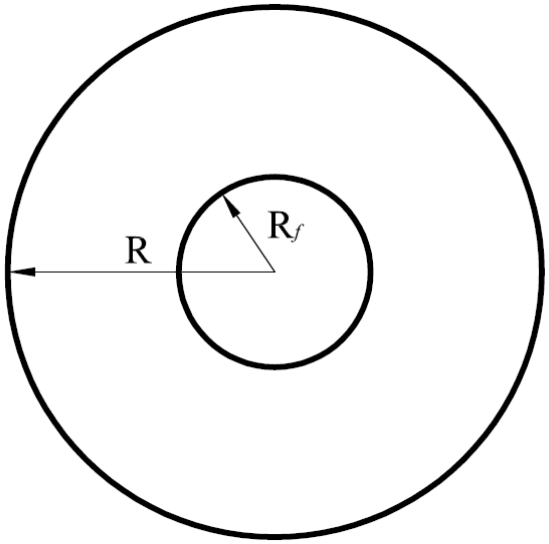

Fig. 2.1.2 Schematization of a 1mm MJR strand

The filaments themselves will be approximated as circles with radius *F*. For the radius the following relation is assumed:

$$\pi F^2 = \frac{Non-Cu\_area}{Number\_of\_filaments} \quad \rightarrow \quad F = 49.9[\mu m]$$

2.2 Volumetric specific heat of Nb_3Sn $T<T_c$

For high fields and temperature below T_c the specific heat of the Nb_3Sn follows the relation [4]:

$$C_{NbSn} = \beta \cdot T^3 + \alpha \cdot T$$

Where α and β are functions of the magnetic field only. At lower fields this relation is valid only for temperatures between ~1.9 and 4.5K; in this temperature range α and β have been parameterized fitting the experimental data by Bouquet [5]:

$$\alpha = \left(4.48 \cdot 10^{-3} B^2 + 4.08 \cdot 10^{-1} B + 9.34 \cdot 10^{-1}\right) \cdot \left[mJ \cdot K^{-2} gat^{-1}\right]$$

$$\beta = \left(6.08 \cdot 10^{-2} \cdot \log\left(11.22 \cdot B + 17\right)\right) \cdot \left[mJ \cdot K^{-4} gat^{-1}\right]$$

The experimental data and the values obtained using the above relations are shown in fig. 2.2.1 and 2.2.2 respectively.
For temperatures higher than 4.5K and fields lower than 10T, this parameterization is not sufficiently accurate.
At 0 and 4 T magnetic field values for temperatures higher than 4.5K, we will use the following parameterizations calculated by fitting experimental data between 4.5K and T_c [4]:

$$C_{NbSn}(0T) = \left\{3.36 \cdot 10^{-1} \cdot T^3 - 1.06 \cdot T^2 + 2.42 \cdot T\right\} \cdot \left[mJ \cdot K^{-1} \cdot gat^{-1}\right]$$

$$C_{NbSn}(4T) = \left\{2.92 \cdot 10^{-1} \cdot T^3 - 1.87 \cdot 10^{-1} \cdot T^2 + 2.83 \cdot T\right\} \cdot \left[mJ \cdot K^{-1} \cdot gat^{-1}\right]$$

For field values between 0-4T and 4-10T we will use a weighted average:

$$C_{NbSn}(B) = C_{NbSn}(4T) \cdot \frac{B}{4} + C_{NbSn}(0T) \cdot \left(1 - \frac{B}{4}\right) \quad 0T<B<4T$$

$$C_{NbSn}(B) = C_{NbSn}(10T) \cdot \frac{B-4}{6} + C_{NbSn}(4T) \cdot \left(1 - \frac{B-4}{6}\right) \quad 4T<B<10T$$

In fig. 2.2.3 and 2.2.4 the experimental data [4] and the values calculated for temperatures higher than 4.5*K* are shown.

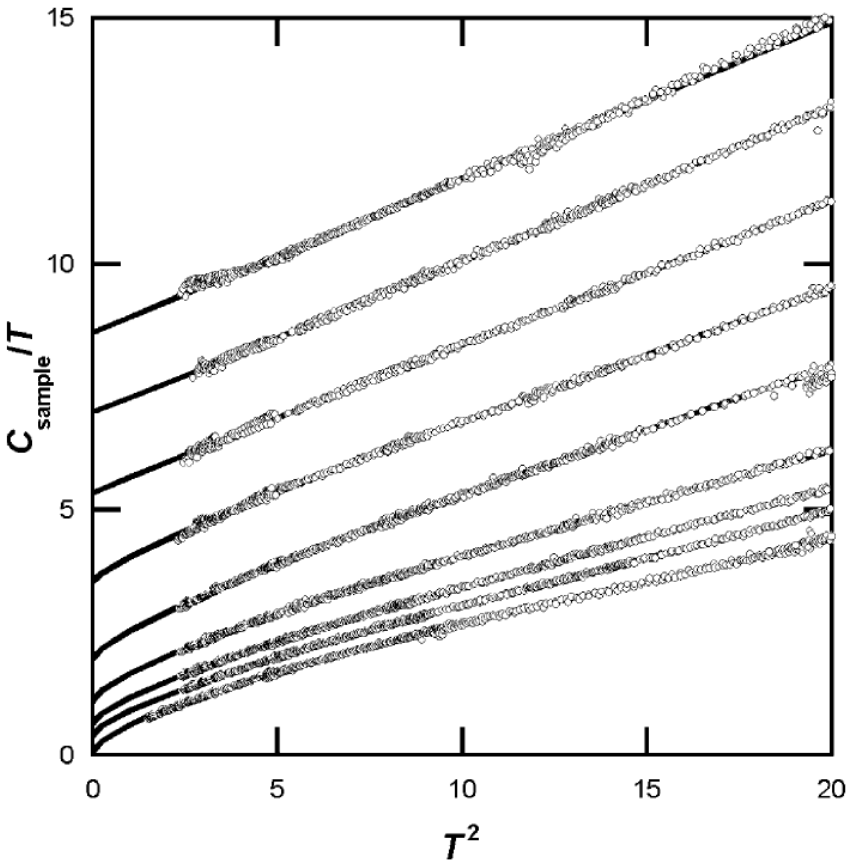

Fig. 2.2.1 Heat Capacity of Nb_3Sn at 0, 0.5, 1, 2, 4, 7, 10, 13, 16 T; experimental data [5]

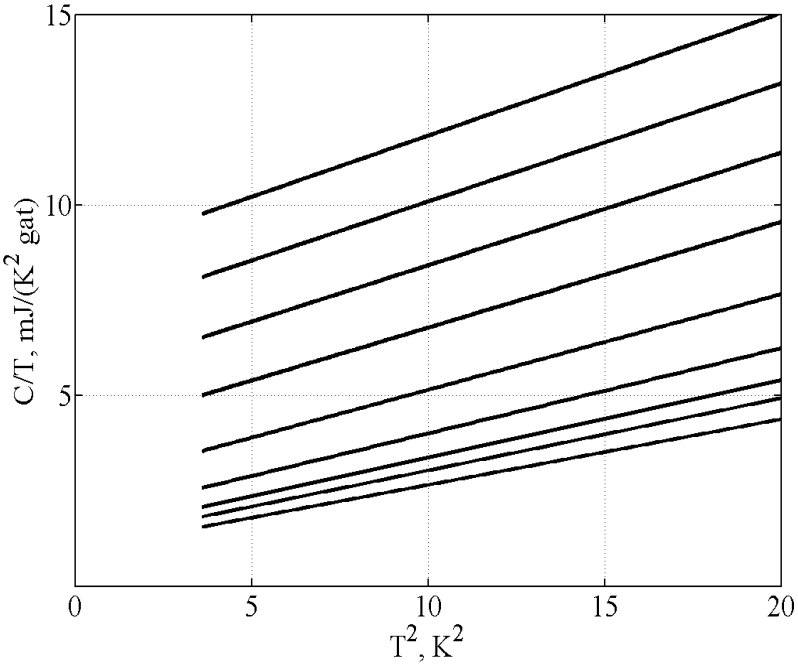

Fig. 2.2.2 Calculated Heat Capacity of Nb_3Sn at 0, 0.5, 1, 2, 4, 7, 10, 13, 16 T

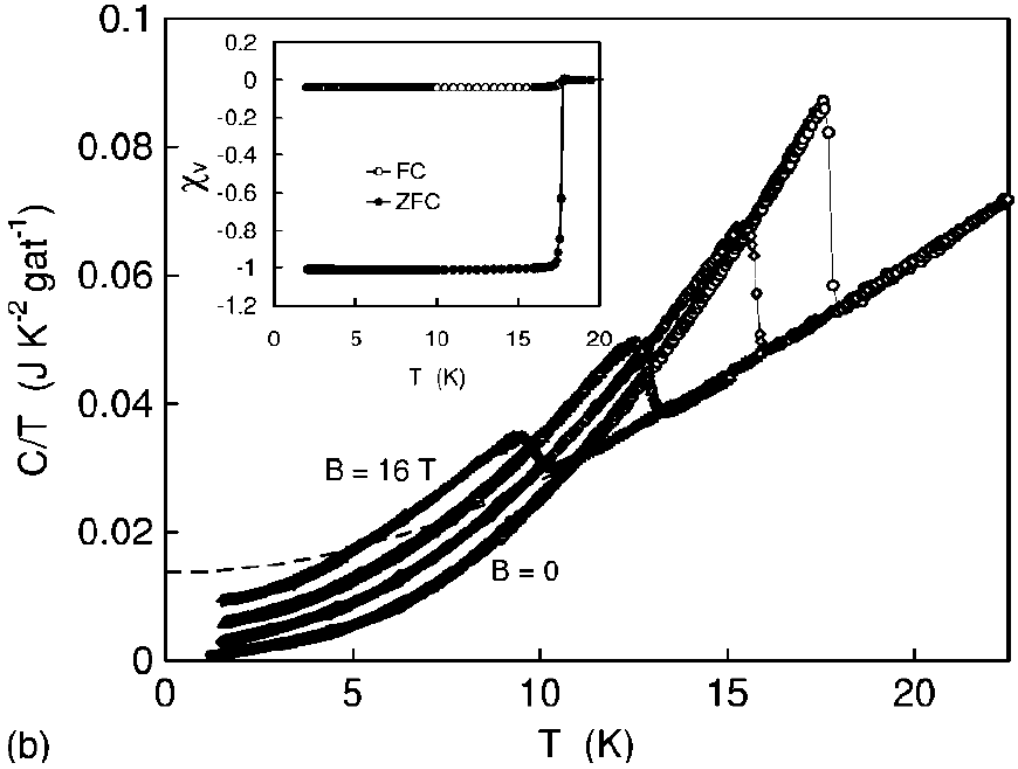

Fig. 2.2.3 Heat Capacity of Nb_3Sn at 0,4,10 and 16 T; experimental data [4]

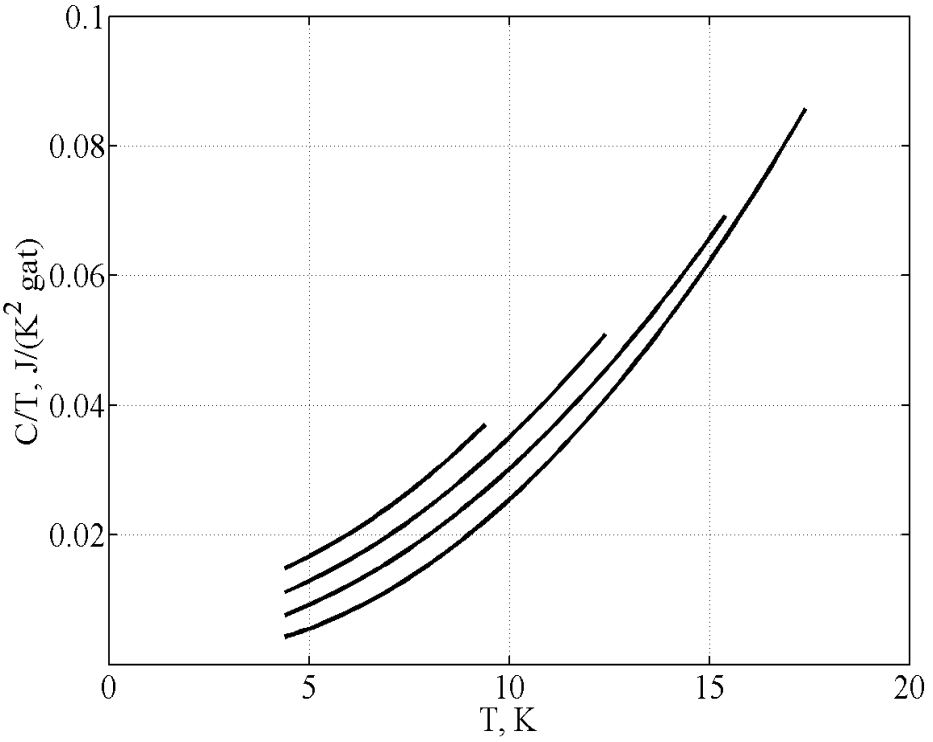

Fig. 2.2.4 Calculated Heat Capacity of Nb_3Sn at 0,4,10 and 16 T

Taking into account that:

$$1gat = 0.25[mole] \qquad 1gat_{NbSn} = 99.5[g] \qquad \rho_{NbSn} = 8910[kg \cdot m^{-3}]$$ [4]

to convert the specific heat value into S.I. units, fig. 2.2.5, we have to introduce for the following multiplication factor:

$$\frac{1mJ}{K \cdot Gat} = \frac{10^{-3} J}{K \cdot 99.5 \cdot 10^{-3} kg} \cdot 8910 kg \cdot m^{-3} = 89.55 \cdot J \cdot K^{-1} \cdot m^{-3}$$

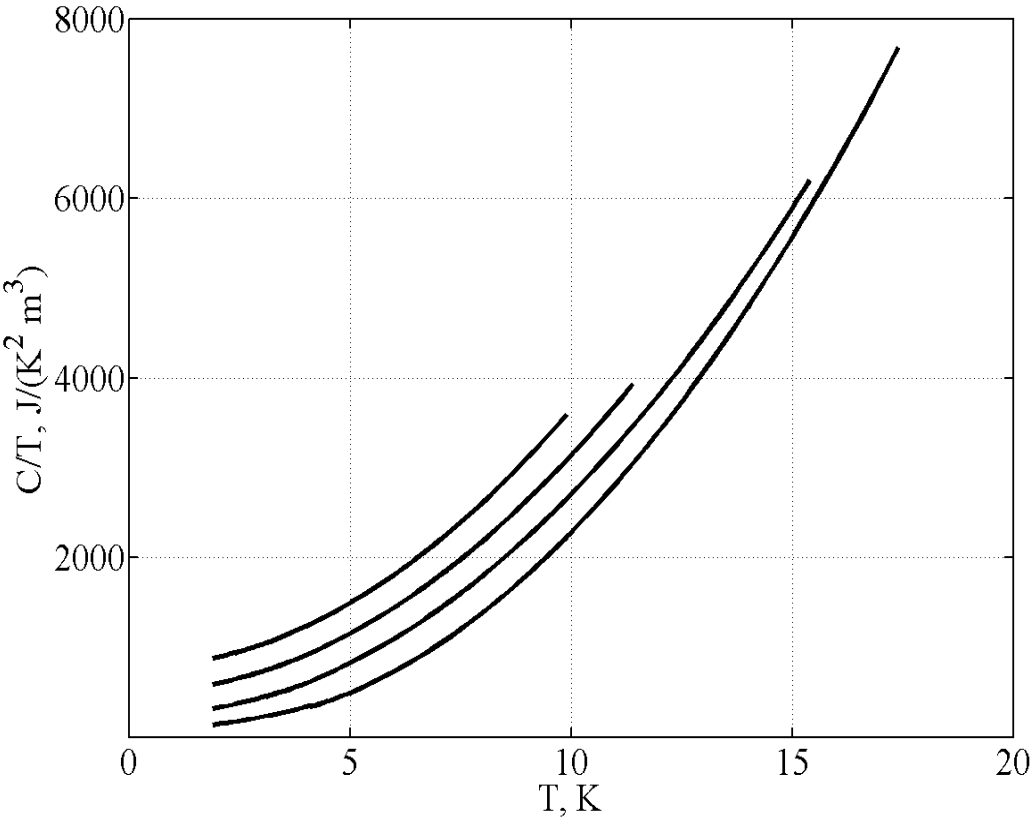

Fig. 2.2.5 Calculated Heat Capacity of Nb_3Sn at 0,4,10 and 16 T

2.3 Volumetric specific heat of the MJR composite $T<T_c$

As seen in the geometry section, the composite is made of Nb_3Sn, copper and bronze. For the volumetric specific heat of copper, the following parameterization will be used:

$$C_{Cu} = 6.8 \cdot T^3 + 97.4 \cdot T \quad [6]$$

The same equation will be also used to calculate the volumetric specific heat of the bronze, considering negligible difference between copper and bronze.
The volumetric specific heat of the composite will be calculated as the average, weighted over the areas, of the volumetric specific heat of each component, from tab. 2-1:

$$C_{comp} = \frac{305}{474} C_{NbSn} + \frac{52}{474} C_{Cu} + \frac{117}{474} C_{Bronze} \approx \frac{305}{474} C_{NbSn} + \frac{52}{474} C_{Cu} + \frac{117}{474} C_{Cu}$$

2.4 Critical current of the 1mm MJR strand

At a fixed temperature the critical current of a MJR strand follows the following parameterization [7]:

$$I_C = C' \cdot B_{pk}^{-0.5} \cdot \left(1 - B_{pk} \cdot B_{C2}^{-1}\right)^2$$

Where the peak field, B_{pk}, in a 1mm MJR strand is [7]:

$$B_{pk} = \max(B_{bg} + 0.413 \cdot 10^{-3} \cdot I,\ 0.648 \cdot 10^{-3} \cdot I - B_{bg})$$

The measured strand, at 4.2*K*, has:

$$C' = 12232.49 \cdot \left[T^{0.5} A\right] \qquad B_{c2} = 22.32 \cdot [T]$$

For a background field of 12 T the critical current was about 705 *A* and the peak field about 12.3 T. Regarding the critical current density:

$$J_C = \frac{I_C}{non\_cu\_area} = \frac{C'}{non\_cu\_area} \cdot B_{pk}^{-0.5} \cdot \left(1 - B_{pk} \cdot B_{C2}^{-1}\right)^2$$

For the 1*mm* MJR geometry presented in 2.1.:

$$\frac{C'}{non\_cu\_area} = \frac{12232.49}{0.422} = 28987 \cdot \left[T^{0.5} A \cdot mm^{-2}\right]$$

This means that the J_c at 12.3 T is about 1670 A/mm^2.

In order to calculate the temperature dependence we will use the following relations [7]:

$$T_c(0) = 18[K] \quad [8]$$

$$I_c(T,\bar{\varepsilon}) = C''\left(1-\left(\frac{T}{T_c(\bar{\varepsilon})}\right)^2\right)^2 \cdot B_{pk}^{-0.5} \cdot \left(1-\frac{B_{pk}}{B_{c2}(T,\bar{\varepsilon})}\right)^2$$

Where:

$$B_{c2}(4.2,\bar{\varepsilon}) = B_{c2}$$

$$B_{c2}(4.2,0) = 28.1\left(1-\left(\frac{4.2}{18}\right)^{1.374}\right) = 24.3[T]$$

$$T_c(\bar{\varepsilon}) = T_c(0)\cdot\left[\frac{B_{c2}(4.2,\bar{\varepsilon})}{B_{c2}(4.2,0)}\right]^{\frac{1}{3}}$$

$$C'' = C'\cdot\left(1-\left(\frac{4.2}{T_c(\bar{\varepsilon})}\right)^2\right)^{-2}$$

$$B_{c2}(0,\bar{\varepsilon}) = B_{c2}(4.2,\bar{\varepsilon})\left(1-\left(\frac{4.2}{T_c(\bar{\varepsilon})}\right)^{1.374}\right)^{-1}$$

$$B_{c2}(T,\bar{\varepsilon}) = B_{c2}(0,\bar{\varepsilon})\left(1-\left(\frac{T}{T_c(\bar{\varepsilon})}\right)^{1.374}\right)$$

3. Magnetization energy stored in the filament

We will consider the case when the superconductor is not magnetized and the external magnetic field is ramped up starting from 0T.
The stored energy of the filament was calculated using the approach developed by Wilson (Wilson book page 133 and 134). According to Wilson the released energy density due to slab magnetization when the field was fully penetrated, fig.3.1, can be obtained by the following formula:

$$dQ = \mu_0 J_c(-dJ_c)\frac{a^2}{3} \qquad (3.1)$$

where $2a$ is the slab thickness. Using this energy density formula one can integrate it over the entire cross section of a circular shaped filament to obtain the total stored energy. In order to do the integration of (3.1) for a circle, a (slab thickness) was introduced as a function of y:

$$\delta Q(y, J_c) = 2a(y)dy \cdot \mu_0 J_c(-dJ_c)\frac{a(y)^2}{3}$$

The next few equations help to follow how the analytical solution for calculating the stored energy was obtained in a case when the field was fully penetrated.

$$a = \sqrt{F^2 - y^2} = F\sqrt{1 - \frac{y^2}{F^2}}$$

$$dQ(J_c) = 2 \cdot \int_0^F \left[2a(y)\mu_0 J_c(-dJ_c)\frac{a(y)^2}{3} \right] dy$$

$$dQ(J_c) = 4 \cdot \frac{\mu_0 J_c(-dJ_c)}{3} \int_0^F a(y)^3 dy$$

$$\int_0^F a(y)^3 dy = F^4 \int_{\frac{\pi}{2}}^0 \cos^4(\alpha) d\alpha = F^4 \frac{3}{16}\pi$$

$$dQ(J_c) = 4 \cdot \frac{\mu_0 J_c(-dJ_c)}{3} F^4 \frac{3}{16}\pi = F^4 \pi \frac{\mu_0 J_c(-dJ_c)}{4}$$

$$Q = \int_{J_c}^0 F^4 \pi \frac{\mu_0 J_c(-dJ_c)}{4} = \frac{\pi \cdot \mu_0}{4} F^4 \frac{J_c^2}{2}$$

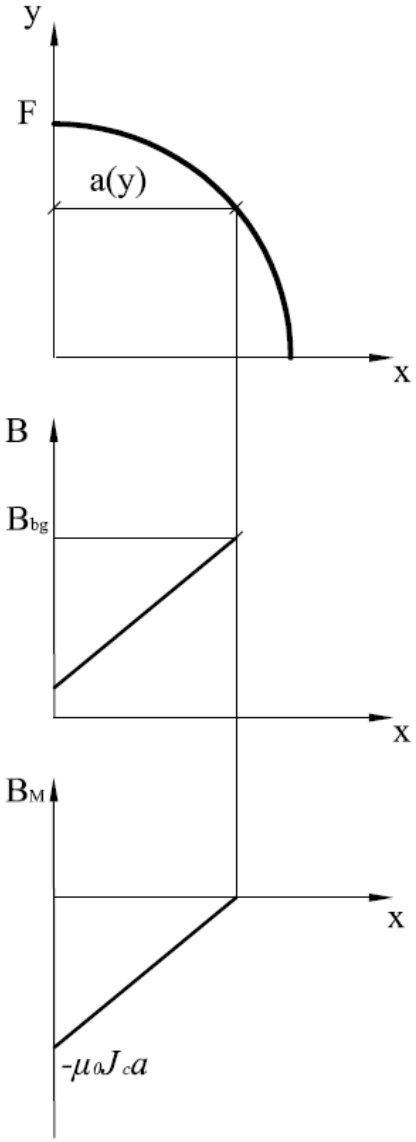

Fig. 3.1 Filament fully penetrated: field distribution

$$\boxed{Q = \frac{\pi^2 \cdot 10^{-7}}{2} F^4 J_c^{\,2}} \qquad (3.2)$$

Es 3T J_c=1.3*10^10 R=50micron (1mm MJR)

$$Q = \frac{\pi^2 \cdot 10^{-7}}{2} R^4 J_c^{\,2} = 5.21 \cdot 10^{-4} \, Joule$$

Since we need to calculate the stored energy even if the field was not fully penetrated another approach was used. The stored energy of the magnetic field is:

$$E = \frac{1}{2 \cdot \mu_0} \int_V B^2 \cdot dV$$

For a circular shaped filament using still the slab approach:

$$E = \frac{1}{2 \cdot \mu_0} 4 \cdot \int_0^R \left\{ \int_0^a B^2 \cdot dx \right\} \cdot dy$$

In order to calculate the above integral we have to make further assumptions. Increasing the background field, the magnetic field penetrates more and more into the superconductor filament. When the field is not completely penetrated, the penetration depth (a_p) can be calculated using the Bean's model, fig. 3.2:

$$a_p = \frac{B_{bg}}{\mu_0 J_c} \;\rightarrow\; a_p \le a$$

The filament will be fully penetrated when the magnetic field reaches the 'total penetration' field (B_p):

$$B_p = \mu_0 J_c a$$

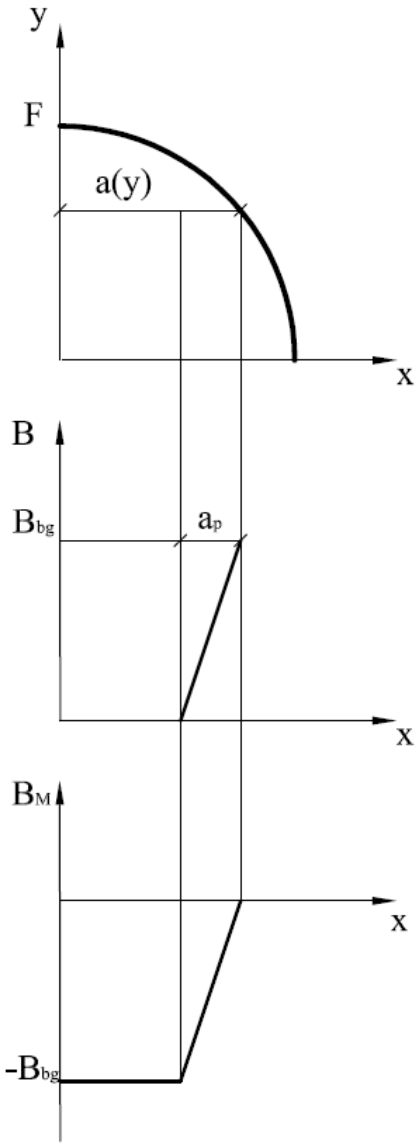

Fig. 3.2 Filament not fully penetrated: field distribution

Making the assumption that the field inside the conductor is cancelled due to magnetization effect the field produced by magnetization (B_M) is:

$$B_M = -B_{bg} \qquad x \le a - a_p$$

$$B_M = -\left\{ B_{bg} - \mu_0 J_c \cdot \left[x - \left(a - a_p \right) \right] \right\} = \mu_0 J_c \left(x - a \right) \qquad x > a - a_p$$

For a case when $B_{bg} > B_p$:

$$B_M = \mu_0 J_c \left(x - a \right)$$

To verify that this approach will give the same result as what we obtained in (3.2.) let us calculate the energy for a filament when the magnetic field is fully penetrated:

$$B_M = \mu_0 J_c (x - a)$$

$$E = \frac{1}{2 \cdot \mu_0} 4 \cdot \int_0^F \left\{ \int_0^a \mu_0^2 J_c^2 (x-a)^2 \cdot dx \right\} \cdot dy$$

$$E = \frac{\mu_0 J_c^2}{2 \cdot} 4 \cdot \int_0^F \left\{ \int_0^a (x-a)^2 \cdot dx \right\} \cdot dy$$

$$E = \frac{\mu_0 J_c^2}{2 \cdot} 4 \cdot \int_0^F \left\{ \frac{(x-a)^3}{3} \Big|_0^a \right\} dy = \frac{\mu_0 J_c^2}{3} 2 \cdot \int_0^F a^3 dy = \frac{\mu_0 J_c^2}{3} 2 \cdot \frac{3}{16} \pi \cdot F^4 = \frac{1}{8} \pi \cdot \mu_0 J_c^2 \cdot F^4$$

$$\boxed{Q = \frac{\pi^2 \cdot 10^{-7}}{2} F^4 J_c^{\,2}}$$

Indeed we obtained the same result.
It is important to point out that this model is not exact since the finite cylindrical shape conductor can not be estimated as a slab so neither the current distribution neither the field distribution is exactly correct. Better value can be obtained by using finite element modeling.

4. Self-field instability: calculation of the 'Self field' energy released by the current redistribution

Due to the self field the transport current flows as close as possible to the strand surface. The current flows at the critical current density of the conductor and it penetrates only as deep as it necessary to carry the transport current, shielding the interior of the conductor from the self-field (Wilson page 141).
Taking as a reference a superconducting strand which has an annular section with an internal radius equal to R_f and an external radius equal to R, fig.4.1, the transport current will flow in the external shell between R and c, where c has to satisfy the following equation:

$$I = \pi(R^2 - c^2)$$

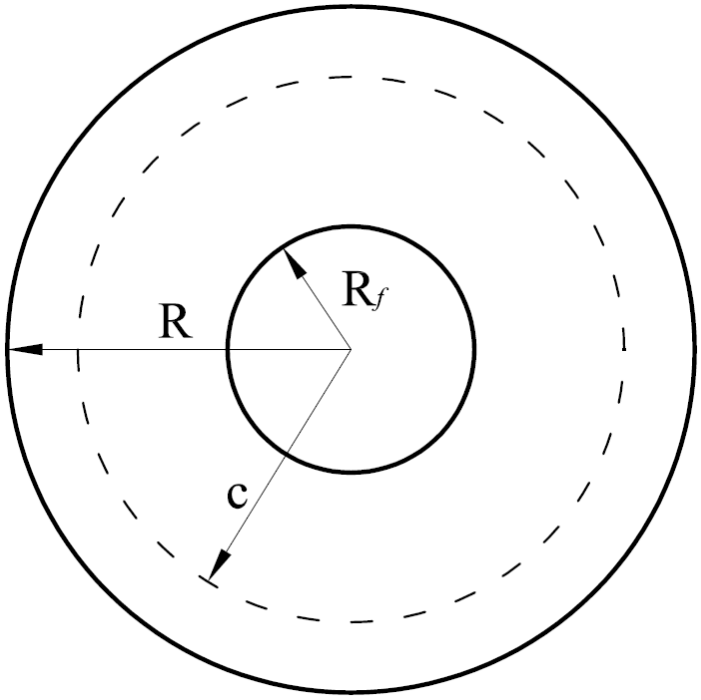

Fig. 4.1 Transport current distribution in a superconducting strand

During self field instability the current redistribute in the superconductor section producing heat.
Based on the assumption that the temperature is uniform in the section of the superconductor where the current flows and $J_c=f(T,B_{peak})$, we will be able to calculate the energy released by a complete redistribution of the transport current.

From page 141 in Wilson book, the released energy for a unit length of a conductor is:

$$dQ = \mu_0 \lambda^2 J_c(-dJ_c) R^4 \pi \left\{ -\frac{1}{2}\ln\varepsilon - \frac{3}{8} + \frac{\varepsilon^2}{2} - \frac{\varepsilon^4}{8} \right\}$$

Where $\varepsilon = {}^{c}\!/_{R}$

$$dQ(t) = \mu_0 \lambda^2 J_c(t)(-dJ_c(t)) R^4 \pi \left\{ -\frac{1}{2}\ln\varepsilon(t) - \frac{3}{8} + \frac{\varepsilon^2(t)}{2} - \frac{\varepsilon^4(t)}{8} \right\}$$

Since the current is constant:

$$\pi\left(R^2 - c^2(t)\right)\lambda J_c(t) = \pi\left(R^2 - c^2(0)\right)\lambda J_c(0) = I$$

$$J_c(t) = \frac{I}{\pi\lambda\left(R^2 - c^2(t)\right)} \qquad dJ_c(t) = \frac{I}{\pi} \cdot \frac{2c(t)}{\lambda\left(R^2 - c^2(t)\right)^2} dc(t)$$

$$dQ(t) = -\mu_0 \lambda^2 \frac{I}{\lambda\pi\left(R^2 - c^2(t)\right)} \frac{I}{\pi} \cdot \frac{2c(t)}{\left(R^2 - c^2(t)\right)^2} dc(t) R^4 \pi \left\{ -\frac{1}{2}\ln\varepsilon(t) - \frac{3}{8} + \frac{\varepsilon^2(t)}{2} - \frac{\varepsilon^4(t)}{8} \right\}$$

$$dQ(t) = -\mu_0 \lambda^2 \frac{I^2}{\pi} \cdot \frac{2c(t)}{\lambda\left(R^2 - c^2(t)\right)^3} dc(t) R^4 \left\{ -\frac{1}{2}\ln\varepsilon(t) - \frac{3}{8} + \frac{\varepsilon^2(t)}{2} - \frac{\varepsilon^4(t)}{8} \right\}$$

$$dQ(t) = -\mu_0 \lambda \frac{I^2}{\pi R^2} \cdot \frac{2c(t)}{\left(1 - \varepsilon^2(t)\right)^3} dc(t) \left\{ -\frac{1}{2}\ln\varepsilon(t) - \frac{3}{8} + \frac{\varepsilon^2(t)}{2} - \frac{\varepsilon^4(t)}{8} \right\}$$

$$dQ(t) = -\mu_0 \lambda \frac{I^2}{\pi a} \cdot \frac{2\varepsilon(t)}{\left(1 - \varepsilon^2(t)\right)^3} dc(t) \left\{ -\frac{1}{2}\ln\varepsilon(t) - \frac{3}{8} + \frac{\varepsilon^2(t)}{2} - \frac{\varepsilon^4(t)}{8} \right\}$$

$$d\varepsilon(t) = {}^{dc(t)}\!/_{R}$$

$$dQ(t) = -\mu_0 \lambda \frac{I^2}{\pi} \cdot \frac{2\varepsilon(t)}{\left(1 - \varepsilon^2(t)\right)^3} d\varepsilon(t) \left\{ -\frac{1}{2}\ln\varepsilon(t) - \frac{3}{8} + \frac{\varepsilon^2(t)}{2} - \frac{\varepsilon^4(t)}{8} \right\}$$

$$Q = -\mu_0 \lambda \frac{I^2}{\pi} \cdot \int_{\varepsilon_o}^{\varepsilon_f} \left[\frac{2\varepsilon}{\left(1 - \varepsilon^2\right)^3} \left\{ -\frac{1}{2}\ln\varepsilon - \frac{3}{8} + \frac{\varepsilon^2}{2} - \frac{\varepsilon^4}{8} \right\} \right] d\varepsilon$$

5 Enthalpy calculation and quench criteria

If the quench current is lower than I_c, the first part of the quench development is characterized by redistribution of the transport current in the composite section. This part of the quench development will end at the time t_f, when the transport current is completely distributed in the whole composite section. At t_f, according to the Bean's model and making the hypothesis that the temperature in the strand section is equal everywhere, the final current density, J_f, has to be:

$$J_f = J_c\left(T_f\right) = \frac{I}{\pi\left(R^2 - R_f^2\right)}$$

Using this relation and the parameterization of the critical current density, we can calculate the temperature, T_f, that the composite must have for a complete redistribution of the transport current.
Once we have this temperature, we can calculate the enthalpy variation per unit length of the composite:

$$\Delta H = \pi\left(R^2 - R_f^2\right)\int_{4.2}^{T_f} C_{comp}\,dT$$

To find out at what transport current value will occur a quench we had to calculate both the enthalpy change value and the released energy (magnetization and self field) value as a function of the transport current. If the two value equal with each other we assume that the sample has quenched. This is obviously an adiabatic model since we assume that during the current redistribution process no heat escapes the conductor.

6 Quench current estimate based on Self field effects

During V-I measurements of the 1 mm MJR strands we observed premature quenches in the low field region (~0-8T). The quench currents were lower than the I_c even if the measurement started with a strand not magnetized. In these conditions the magnetization energy stored in the filaments at the moment of the quench was negligible. The cause of the instability, during these measurements, is most likely the self field energy.
In this chapter we will show and discuss the quench current calculated by the adiabatic model considering the amount of energy released during the current redistribution equal to the stored self field energy (chapter 4).
The results of the calculations are summarized in fig.6.1; at low magnetic fields the quench current estimated by the model is much lower than the critical current, this difference gets smaller by increasing the magnetic field. In fig. 6.2 the self field energy and the enthalpy margin are shown as a function of the current for different magnetic fields. At the current level where the two curves cross each other, the sample may quench due to self field instability.

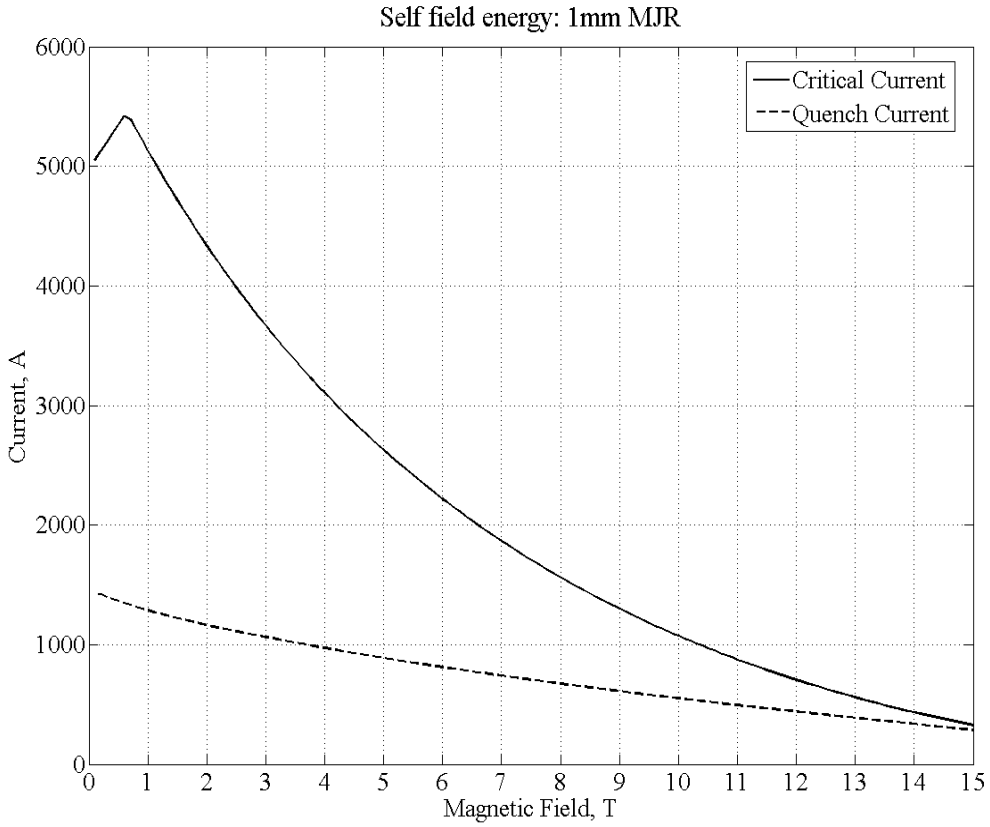

Fig. 6.1 Quench current estimate based on self field effect

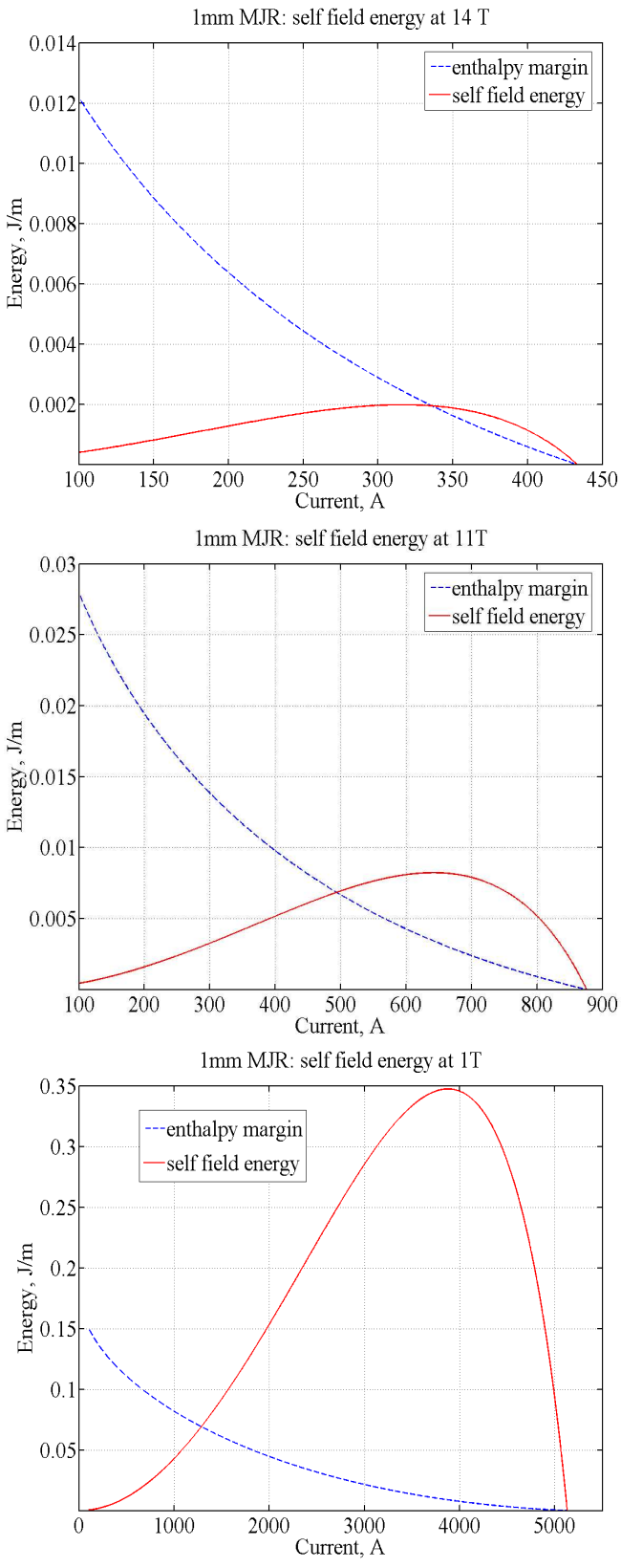

Fig. 6.2 Self-field energy and enthalpy margin for different magnetic fields

7 Quench current estimate based on Self field and Magnetization effect

During V-H measurement the strand is strongly magnetized and the magnetization energy can not be neglected in calculating the quench current. In this paragraph we present the quench current values obtained by the model taking in to account that, during the current redistribution, both, the self field and magnetization energy are released.
The magnetization energy is calculated for the case where the background magnetic field is ramped up from 0T starting with a strand not magnetized. In these conditions the magnetization energy stored in a filament can be calculated using the equation presented in chapter 3. The total amount of magnetization energy is calculated by multiplying the magnetization of a single filament by the total number of filaments and by the fraction of the composite area not occupied by transport current.
These results are summarized in fig. 7.1. At high field values the quench current is almost the same as what was obtained by taking into account in the calculation the self field energy (for field higher than 4T the difference is less than 15%) only. However, at lower field values there is a significant difference. In particular around 1.2T the quench current has a minimum, it is almost by factor of two less than what was calculated for the self field case.

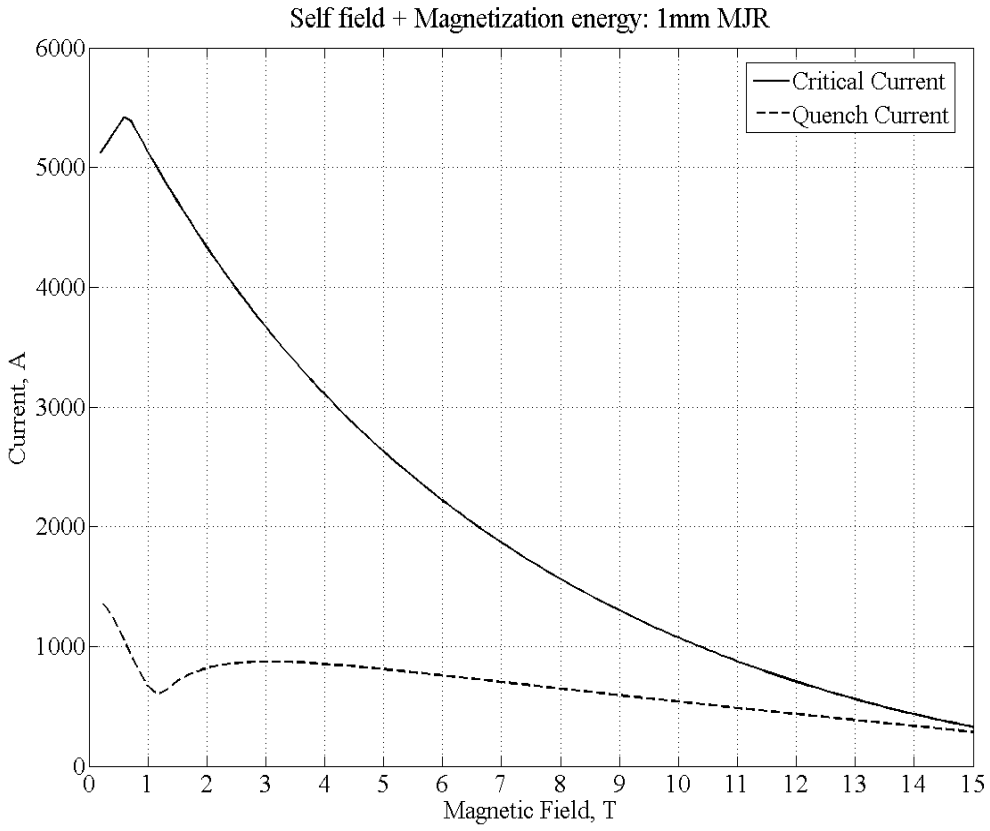

Fig. 7.1 Quench current estimate based on self field and magnetization effect

8 Self Field in a strand cross section of the coil like sample

In this chapter we estimate the value of the self field in the strand cross section of the coil like sample. This cross section is the intersection between the coil and the plane passing through the axis of the coil, fig. 8.1.
The value of the self field inside a cross section of a strand can be described as the superimposition of two components: the first one, B_{coil}, magnetic field from other part of the coil; the second component, B_j, dependent on the distribution of the current density in the strand cross section under examination.

$$\vec{B}_{sf} = \vec{B}_{coil} + \vec{B}_j$$

We will assume that the strand cross section is circular, the current density is everywhere perpendicular to the cross section and its value is only function of r, which is the distance from the center of the circle. With this hypothesis B_j has only tangential component and its value is:

$$B_j = \frac{\mu_0}{2\pi \cdot r} I(r) \qquad (8.1)$$

where $I(r)$ is the total current in the circular area with radius r.
The B_{coil} has mainly a z component and it is anti parallel to the background field generated by the external solenoid magnet, fig.8.1
Taking into account only the z component of the field (see fig 8.1), from a finite element analysis of a composite strand with a radius of 0.4 mm:

$$B_{sf}(a) = -0.648 \cdot 10^{-3} I = B_{Coil}(a) + B_j(a)$$

$$B_{sf}(b) = 0.414 \cdot 10^{-3} I = B_{Coil}(b) + B_j(b)$$

From eq 8.1

$$B_j(a) = -\frac{4\pi \cdot 10^{-7}}{2\pi \cdot 0.4 \cdot 10^{-3}} I(r) = -0.5 \cdot 10^{-3} \cdot I$$

$$B_j(b) = 0.5 \cdot 10^{-3} \cdot I$$

Substituting:

$$B_{Coil}(a) = -0.648 \cdot 10^{-3} I - B_j(a) = -0.648 \cdot 10^{-3} I + 0.5 \cdot 10^{-3} \cdot I = -0.148 \cdot 10^{-3} \cdot I$$

$$B_{Coil}(b) = 0.414 \cdot 10^{-3} I - B_j(a) = 0.414 \cdot 10^{-3} I - 0.5 \cdot 10^{-3} \cdot I = -0.086 \cdot 10^{-3} \cdot I$$

We will make the following simplification. The field due to the coil itself at a particular location of the strand is constant and equal to the arithmetic average between the above described extreme points:

$$\hat{B}_{Coil} = -\frac{0.148 + 0.086}{2} \cdot 10^{-3} \cdot I = -0.117 \cdot 10^{-3} \cdot I$$

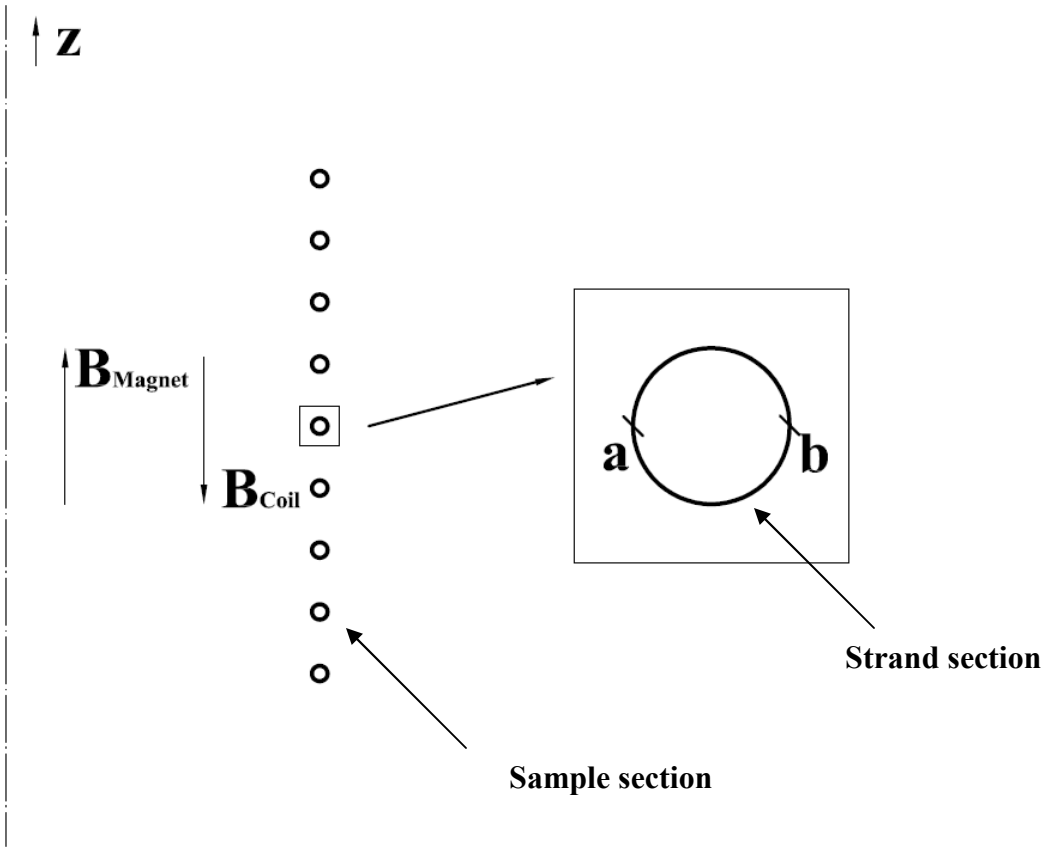

Fig. 8.1 Cross section of the sample

9 Magnetization in the coil like sample due to self field

Up to now, in the calculation of the magnetization energy, we neglected the magnetic field generated by the coil itself. The B_{coil} self-field component described in the previous chapter should be treated as a background field consequently it increases the calculated value of the strand magnetization.

In V-I measurements (starting with the sample not magnetized), by ramping up the current the strand gets slightly magnetized due the filed change induced by the adjacent coil turns.

To take into account this effect in the model, the magnetization energy produced by the variation of the self field from 0 to B_{coil} has to be added to the self-field energy.

The self-field plays a role in V-H measurements as well since any current change will induce a magnetization as it was described above. Because of the self field, when we start to ramp up the field from 0T with transport current, the sample it is slightly magnetized even if it was not magnetized before ramping up the current.

If we ramp up the magnetic field from 0 T under a transport current the magnetization direction due to self field has opposite sign relative to the magnetization due to the background field up ramp. This means that initially, the background field will reduce the magnetization due to self field. When the field generated by the magnet is bigger than two times of B_{coil} , the distribution of the persistent current is practically the same as if the strand had been subjected to an external field increasing from 0T to B_{Magnet}-B_{Coil}. In this case the magnetization energy can be calculated by using the same formulation as it was used previously by substituting B_{bg} with B_{Magnet}-B_{Coil}. The magnetization energy for B_{Magnet}-$=0$ is due to self-field.

Since for 0T < B_{Magnet} < 2 B_{coil} , the calculation of the magnetization energy is a little more complicated and since the B_{coil} value is quite small, we decided not to calculate I_q in this range.

. In fig. 9.1 the quench current estimate is shown with and without taking into account the contribution of the magnetization energy due to self field effect in the coil like sample.

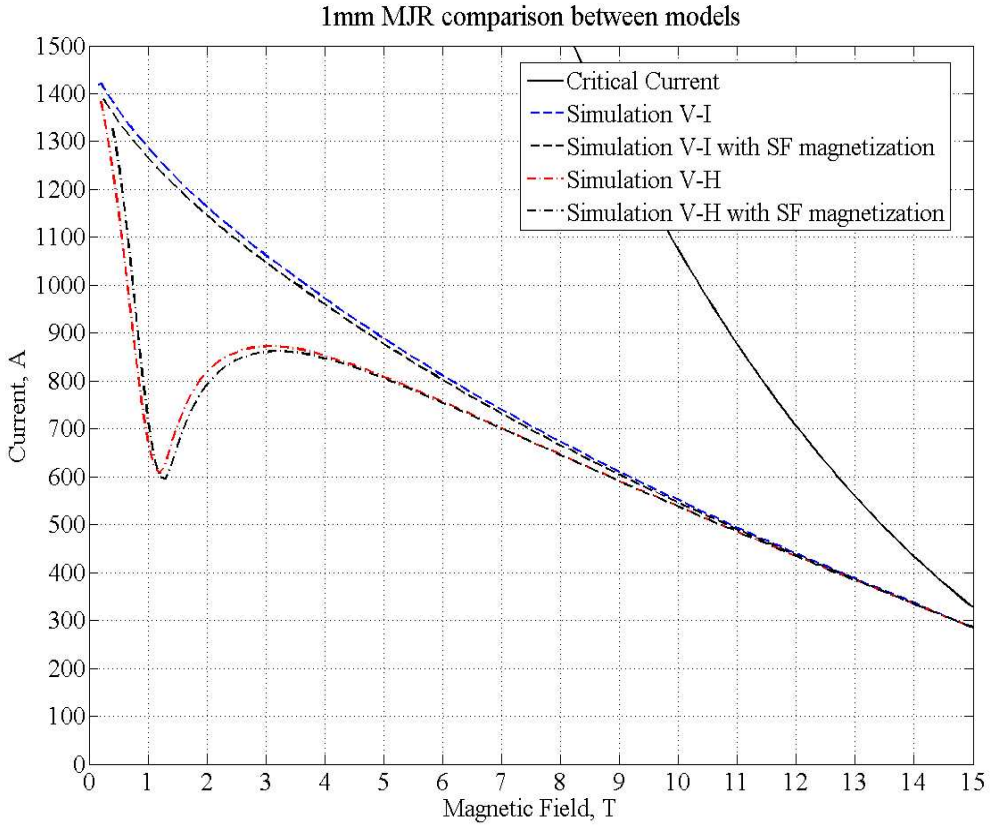

Fig. 9.1 Effect of the magnetization produced by the self-field

10 Comparison with experimental results

In this chapter we will show a comparison between the quench current estimated by the model and the results that we had obtained measuring a 1 mm MJR strand with a low RRR copper matrix (7). This sample is a good candidate for this adiabatic approach because of the low thermal and electrical conductivity of the copper matrix which does not allow large amount of energy to diffuse outside of the composite.
The calculations presented in chapter 6 simulates the quench currents during V-I measurements starting with a sample not magnetized, while the calculations in paragraph 7 are the simulation of V-H measurements starting from 0T with the sample not magnetized. The experimental data in these physical conditions are showed in fig. 10.1 and compared with analytical simulations.
The adiabatic model fits quite well the experimental data at fields lower than 6T, while it underestimates significantly the quench current at higher field values. This is probably due to the fact that the amount of energy that diffuses outside the composite (dynamic effect) during instability is not negligible at high field.
At high field the energies associated with thermo-magnetic instabilities are very small, this means that even small energy diffusion can prevent a premature quench of the strand. For example during V-I measurements at 11T the maximum energy associated with the instability is less than 10 mJ/m, fig.6.2; an energy diffusion of that order of magnitude can prevent the strand from premature quenching.
On the other hand, looking at fig. 6.2, we can see that the same amount of energy will not have any significant effect in the quench current value during V-I measurement at 1T.

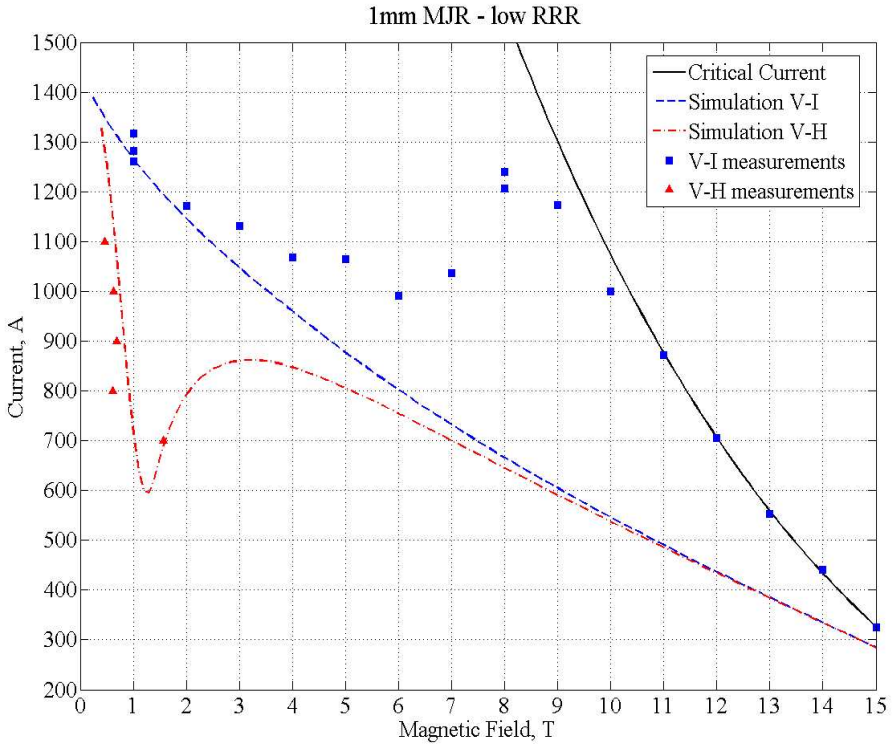

Fig. 10.1 Comparison between model and experimental data

References

[1] B. Bordini S. Feher, Fermilab Technical Note 05-029

[2] B. Bordini S. Feher, Fermilab Technical Note 06-016

[3] B. Bordini et al. – "Voltage Spikes in Nb_3Sn and NbTi strands" – IEEE Trans. Appl. Superconduct., presented at MT 19 and to be published in 2006

[4] Guritanu *et al.*Phys. Rev. B 70, 184526 (2004)

[5] Bouquet *et al.*, Physica C 408-410 (2004) 60-62.

[6] M. S. Lubell, IEEE Trans. Mag-19 (1983) 754

[7] B. Bordini S. Feher, Fermilab Technical Note 05-028

[8] S. A. Keys D. P. Hampshire, Supercond. Sci. Technol., Vol 16, pag. 1097, 2003